Cell Reports
Physical Science

CellPress
OPEN ACCESS

Article

Combined computational-experimental study of Ru(0)-catalyzed Guerbet reaction

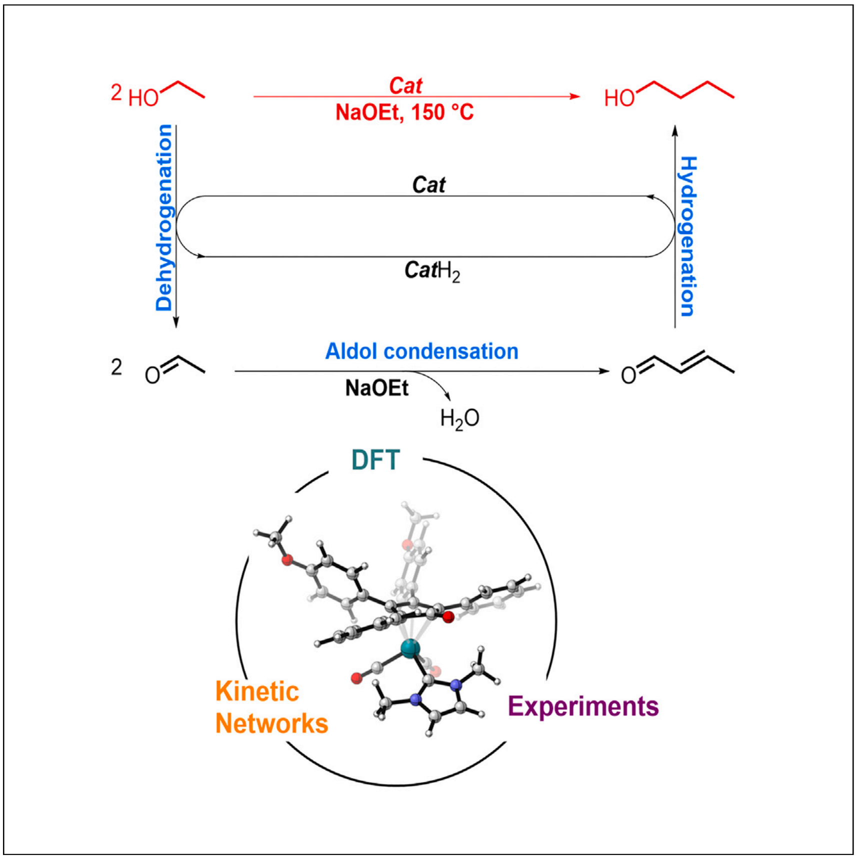

Calcagno et al. show the reaction performance of a ruthenium catalyst for the production of biofuels from second-generation feedstock. Synergistic experimental and computational investigations provided fundamental insights into the key factors governing the complex reaction mechanism, paving the way for strategies for the rational design of new catalysts.

Francesco Calcagno, Cristiana Cesari, Anna Gagliardi, ..., Fahmi Himo, Rita Mazzoni, Ivan Rivalta

fahmi.himo@su.se (F.H.)
rita.mazzoni@unibo.it (R.M.)
i.rivalta@unibo.it (I.R.)

Highlights

A recyclable Ru(0)-NHC homogeneous catalyst for the Guerbet reaction is reported

Reaction mechanism was elucidated with a synergistic approach

Microkinetic simulations disclosed key steps for selectivity and conversion

Role of H_2 production was elucidated and new strategies for catalyst design proposed

Calcagno et al., Cell Reports Physical Science 5, 102291
November 20, 2024
https://doi.org/10.1016/j.xcrp.2024.102291

Please cite this article in press as: Calcagno et al., Combined computational-experimental study of Ru(0)-catalyzed Guerbet reaction, Cell Reports Physical Science (2024), https://doi.org/10.1016/j.xcrp.2024.102291

Cell Reports
Physical Science

CellPress
OPEN ACCESS

Article

Combined computational-experimental study of Ru(0)-catalyzed Guerbet reaction

Francesco Calcagno,[1,2] Cristiana Cesari,[1,2] Anna Gagliardi,[1,2] Alessandro Messori,[1,2] Andrea Piazzi,[1,2] Filippo Tamassia,[1] Marco Garavelli,[1] Fahmi Himo,[3,*] Rita Mazzoni,[1,2,*] and Ivan Rivalta[1,2,4,5,*]

SUMMARY

The homologation of bioethanol to higher alcohols by means of the Guerbet reaction is a promising way to obtain biofuels. Herein, we present an efficient ruthenium-catalyzed process and a detailed investigation of the reaction mechanism using a combined experimental-computational approach. Density functional theory calculations of the free energy profiles are corroborated by designed experiments. Microkinetic simulations are performed based on the calculated energies, providing good agreement with experimental observations of the time-evolving ethanol conversion and product distribution. Analysis of the kinetics network elucidates the key steps governing the conversion and selectivity of the Guerbet process, pointing out the unexpected role of the molecular hydrogen evolution step and suggesting strategies to design new catalysts for the Guerbet reaction.

INTRODUCTION

Biofuels from second-generation feedstock are promising to tackle the climate change challenge, being an appealing alternative to fossil fuels. Branched and linear alcohol mixtures with similar characteristics to gasoline and high energy density can be ideally obtained by means of the so-called Guerbet reaction (Scheme 1A),[1,2] enabling the catalytic upgrading of bioethanol to 1-butanol and higher alcohols.[3–5]

Many efforts have been made to improve the conversion of ethanol and the yield and selectivity of 1-butanol by investigating the activity of both heterogeneous[6] and homogeneous[7,8] catalysts.[9] As reported by Wass and co-workers,[7] homogeneous organometallic complexes show mild reaction conditions and good control of yields and selectivity. Although several studies on iridium-,[10] ruthenium-,[11–16] and manganese-based[17,18] catalysts provided insights into the Guerbet reaction,[19–22] the detailed reaction mechanism still remains unknown.[7,8] Disclosing the reaction mechanism might unlock rational design strategies, paving the way for new catalyst candidates.

The overall mechanism of the Guerbet reaction, as described by Veibel and Nielsen,[23] consists of three main steps: (1) dehydrogenation of ethanol by a hydrogen transfer catalyst that produces acetaldehyde, (2) off-cycle aldol condensation between ketones species (catalyzed by a basic co-catalyst) to form an α,β-unsaturated aldehyde (i.e., crotonaldehyde) and water, and (3) double hydrogenation of the aldehydic compound by two molecules of the hydrogenated catalyst to form 1-butanol (Scheme 1A).[23] The homologation to higher alcohols is expected to follow the same reaction mechanism. As simple in theory as it is challenging in practice, the Guerbet reaction efficiency is largely affected by catalyst deactivation and side

[1]Department of Industrial Chemistry "Toso Montanari", University of Bologna, Via Piero Gobetti 85, 40129 Bologna, Italy

[2]Center for Chemical Catalysis – C3, University of Bologna, Via Piero Gobetti 85, 40129 Bologna, Italy

[3]Department of Organic Chemistry, Arrhenius Laboratory, Stockholm University, 106 91 Stockholm, Sweden

[4]ENSL, CNRS, Laboratoire de Chimie UMR 5182, 46 Allée d'Italie, 69364 Lyon, France

[5]Lead contact

*Correspondence: fahmi.himo@su.se (F.H.), rita.mazzoni@unibo.it (R.M.), i.rivalta@unibo.it (I.R.)

https://doi.org/10.1016/j.xcrp.2024.102291

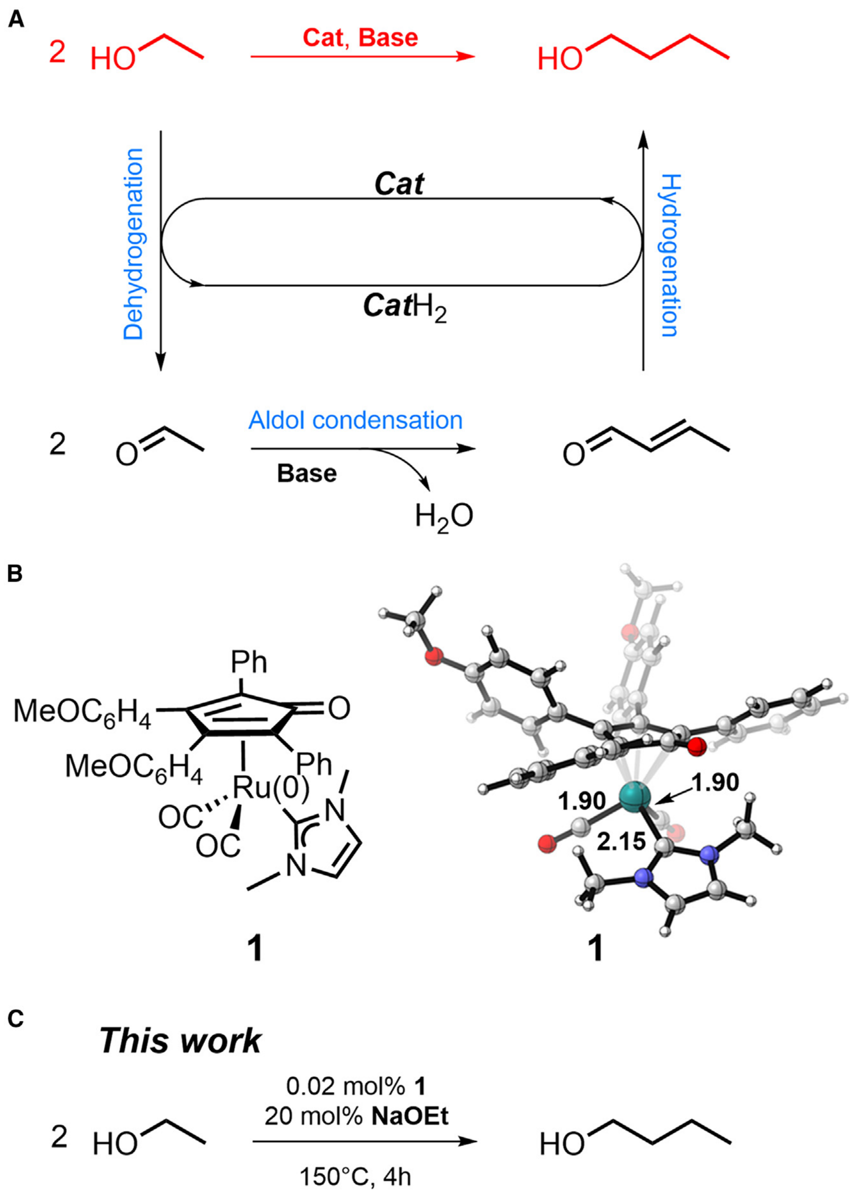

Scheme 1. The Guerbet reaction scheme

(A) General reaction scheme for the Guerbet reaction in basic conditions.

(B) Chemical structure and DFT optimized geometry of catalyst **1** at B3LYP/6-31G(d,p)/LANL2DZ level of theory.

(C) Optimal reaction conditions found in this work.

processes, such as the Cannizzaro and Tishchenko reactions,[24] and molecular hydrogen production.[13,14,23,25]

To the best of our knowledge, only one computational mechanistic investigation has been reported previously for a Mn-catalyzed Guerbet reaction in the homogeneous phase,[26] suggesting a mechanism that is in line with experiments,[17] but without discussing the roles of possible intermediates and resting species involved in various competing reactive pathways as well as that of molecular hydrogen evolution.

Ruthenium-based complexes are well known for being active in hydrogen-borrowing processes,[27–30] being thus far the leading candidates for the Guerbet reaction.[7,8] Mazzoni and co-workers recently reported an ionic carbonyl ruthenium catalyst where the organometallic anion works in tandem with a 1,3-dimethyl imidazolium cation, showing promising performance in the homologation of ethanol.[13,14,31] However, for industrial applications of the reaction, easy-to-functionalize ancillary ligands are desired to promote the heterogenization of homogeneous catalysts. Heterogenized catalysts take advantage of both the efficiency of homogeneous compounds and the higher industrial feasibility of heterogeneous systems in terms of environmental impact and economical sustainability. Among others, N-heterocyclic carbene (NHC) ligands are good candidates since they can be functionalized to immobilize organometallic catalysts in polymers.[32,33] Notably, NHC moieties, ubiquitous as ancillary ligands for homogeneous catalysis due to their versatility and easy way of synthesis,[34–36] have not been employed yet in the Guerbet reaction. In this context, Mazzoni and co-workers developed a ruthenium(0) cyclopentadienone (CpO) complex bearing an NHC ligand (**1**; Scheme 1B).[34] Since these kinds of ruthenium NHC complexes are fairly active in both hydrogenation and dehydrogenation,[37–39] complex **1** constitutes a promising candidate for the catalytic homologation of ethanol to 1-butanol and higher linear and branched alcohols in the presence of a base co-catalyst in the homogeneous phase.

In the present work, we demonstrate that **1** is an excellent catalyst for the Guerbet reaction in the presence of sodium ethoxide as a base co-catalyst (Scheme 1C). Prompted by the novelty of the catalyst, we carried out a combined experimental-computational investigation to elucidate the detailed reaction mechanism of the process. Given the complexity of the reaction mechanism, numerical kinetic simulations have also been carried out based on the free energies computed with density functional theory (DFT), allowing direct comparison with experimental kinetic data. Kinetic simulations in homogeneous catalysis provide insights into the role of each reaction step, disclosing the origin of experimentally observed product distribution and selectivity, allowing for a sensitivity analysis to be performed that could pave the way to designing more efficient catalysts.

RESULTS

In the following, we will first present the experimental catalytic activity of **1** and the reaction condition optimization. Then, we will discuss in detail the three main reaction steps as reported in Scheme 1A,[23] presenting our combined experimental-computational investigations. Since the evolution of molecular hydrogen has been experimentally observed during the Guerbet reaction, the analysis of the reaction mechanism will also account for such a fourth reaction step. Next, kinetics simulations based on the free energies computed with DFT will provide a direct comparison between experimental and theoretical ethanol conversion and distribution of products. Finally, a sensitivity analysis will be reported, shedding light on the key reaction steps and side processes governing the selectivity.

Reaction condition optimization and product distribution

The Guerbet reaction catalyzed by ruthenium(0)-NHC complex **1** in the presence of sodium ethoxide (co-catalyst) was carried out in a Schlenk bomb at autogenous pressure in an inert atmosphere and without adding either an external source of hydrogen or an additional solvent, as ethanol is both the medium and the source of hydrogen (Scheme 1A). Screening of the reaction conditions, namely the catalyst and base co-catalyst loadings, reaction time, temperature, enlarged feedstock (Table 1), and

Table 1. Optimization of the Guerbet reaction conditions

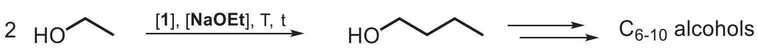

Entry	1 (mol %)	NaOEt (mol %)	EtOH (mL)	Time (h)	T (°C)	Conversion EtOH (%)	Yield BuOH (%)	Yield (C_{4-10}) (%)	C-loss (%)	Selectivity (C_{4-10}) (%)
1	–	20	0.5	4	150	6	<1	<1	<6	<1
2	0.2	–	0.5	4	150	<1	<1	<1	<1	–
3	0.2	10	0.5	4	150	41	28	36	5	88
4	0.2	20	0.5	4	150	53	36	47	6	89
5	0.2	40	0.5	4	150	68	34	49	19	72
6	0.02	5	0.5	4	150	32	16	25	7	78
7	0.02	10	0.5	4	150	44	25	38	6	86
8	0.02	20	0.5	4	150	58	30	50	8	86
9	0.01	5	0.5	4	150	30	13	21	9	70
10	0.01	10	0.5	4	150	48	23	38	10	79
11	0.01	20	0.5	4	150	60	27	47	13	78
12	0.02	20	0.5	0.5	150	20	16	20	<1	>99
13	0.02	20	0.5	2	150	50	31	50	<1	>99
14	0.02	20	0.5	24	150	68	33	60	8	88
15	0.01	20	0.5	2	150	25	16	24	<1	96
16[a]	0.01	20	0.5	16	150	55	25	47	8	85
17	0.02	20	5	4	150	45	29	43	2	96
18	0.02	20	30	4	150	48	28	42	6	88
19	0.01	20	5	4	150	28	21	26	2	93
20	0.01	20	5	16	150	51	28	46	5	90
21	0.2	20	0.5	8	150	58	33	49	9	84
22	0.2	20	0.5	4	120	16	12	14	2	88

The conversion of ethanol, the yield and selectivity of products, and the carbon loss are reported with different reaction conditions.
[a]Maximum turnover number (TON) value of 4,700.

reactivity toward a real matrix (i.e., waste ethanol from the head and tails of ethanol distillation [kindly provided by CAVIRO S.p.a.]; see Table S1), was done to improve the reaction performances.

Two control experiments were carried out: (1) without ruthenium(0)-NHC catalyst **1** (entry 1, Table 1) and just in the presence of 20 mol % sodium ethoxide, showing a low conversion of ethanol (6%) and a negligible yield of 1-butanol (<1%) after 4 h, and (2) in the absence of the base (entry 2, Table 1) with negligible conversion. Instead, in the presence of 0.2 mol % **1** and 20 mol % NaOEt, 53% converted ethanol and a 36% yield of 1-butanol were recorded (entry 4, Table 1).

Lowering the catalyst loading to 0.02 or 0.01 mol % (entries 8 and 11, Table 1) while keeping the same amount of base co-catalyst surprisingly improves the conversion of ethanol, which increases to 58% or 60%, respectively. The total yield of alcohols does not vary much (47% for 0.2 mol % **1** vs. 50% for 0.02 mol % **1** and 47% for 0.01 mol % **1**), while the selectivity to total alcohols decreases from 89% to 86% and 78%, respectively. These trends show that when the concentration of **1** is lowered, more ethanol is converted to something other than alcohols.

Cannizzaro and Tishchenko reactions also have to be taken into consideration[24] since they are well-known side processes running in such conditions.[13] It is indeed known that acetaldehyde conversion to acetate in water, having the aldehyde of an alpha-H atom (which favors aldol condensation), occurs, with a possible role of a related borrowing hydrogen catalyst as previously defined by Milstein et al.[40] This behavior could be a consequence of the Ru-catalyzed direct dehydrogenation of the alcohol or aldehyde in the presence of base and water (which is formed in the reaction), leading to acetate and, therefore, consuming the base as mechanistically described by Dumeignil, Gauvin, and co-workers.[41] The same role of a hydrogen-borrowing catalyst, this time as the related Shvo complex supporting the use of a non-stoichiometric base, was disclosed for the Tishchenko reaction by Gusev and Spasyuk.[42] Under Guerbet conditions, as the produced ester will then consume 1 equiv of the base in the saponification, the acetate is then formed anyway.

To elucidate the presence of the acetate side product, the crude was characterized and quantified working under the selected reaction conditions reported in Table 1 (entry 4). The water-soluble fraction of the solid at the end of the reaction was weighted and analyzed by ^{1}H-nuclear magnetic resonance (^{1}H-NMR), detecting only sodium acetate and sodium butanoate (Figure S1). This outcome is in line with previous statements, confirming that NaOEt is quantitatively converted into acetates.[8,13,14,31]

Keeping a constant concentration of **1**, decreasing the base loading has a negative effect on both conversion and alcohol yield (entries 3–5, 6–8, and 9–11, Table 1), while a significant increase of the base loading (entry 5, Table 1) negatively affects the overall selectivity. In particular, the higher the concentration of the base, the higher the carbon loss of the process (e.g., 19%, entry 5, Table 1), as defined in the supplemental information. This shows that the base plays a fundamental role as co-catalyst but that its concentration should be not so high as to let the Cannizzaro and Tishchenko reactions be competitive with the Ru Guerbet catalysis.

As expected, the reaction temperature is also a key factor in the Guerbet reaction. Below 150°C, the overall reaction rate is slow, and no noticeable yields are recorded (entry 22, Table 1). The reaction time is crucial for the selectivity issue. In fact, the

Table 2. Experimental time-evolving product distribution at selected reaction conditions

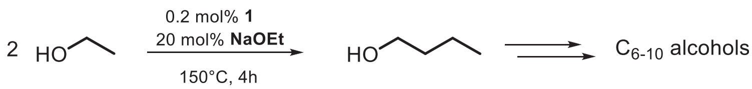

Entry	Time (min)	Conversion EtOH (%)	Yield BuOH (%)	Yield ($C_{4\text{-}10}$) (%)	Yield H_2 (%)	C-loss (%)	Selectivity ($C_{4\text{-}10}$) (%)
1	15	21	17	20	4	1	95
2	30	34	27	32	14	2	94
3	60	42	31	38	17	4	90
4	120	48	35	44	24	4	92
5	180	50	35	44	29	6	88
6	240	53	36	47	29	6	89
7	480	58	33	49	29	9	84

The conversion of ethanol, the yield and selectivity of products, and the carbon loss are reported with different reaction times at selected reaction conditions.

longer the reaction time, the lower the selectivity to total detectable alcohols (entries 12–14, Table 1).

Running the reaction for 30 min (entry 12, Table 1) or 2 h (entry 13, Table 1) gives >99% selectivity, while running it for 24 h (entry 14, Table 1) gives 88%. The decrease in selectivity to total alcohols could be due to the formation of uncharacterized long-chain alcohols, i.e., C_N with N > 10 (that are not counted in the overall alcohol selectivity). The consecutive nature of the Guerbet reaction and thus the presumed impact on selectivity of uncharacterized C_N alcohols over time are confirmed by the improvement of selectivity to $C_{6\text{-}10}$ alcohol. Namely, the selectivity increases from 20% at 30 min to 38% and 40% at 2 and 4 h, respectively (entries 12, 13, and 14, Table 1).

The reaction scale does not affect either the conversion or the selectivity significantly (entries 4, 17, and 18, Table 1). By keeping constant the loadings of **1** and sodium ethoxide but increasing the volume of ethanol from 0.5 (entry 4, Table 1) to 5 (entry 17, Table 1) to 30 mL (entry 18, Table 1), the conversion ranges between 45% and 53%, with an overall selectivity to alcohols between 88% and 96%. It is positively surprising that by scaling up the reaction from 0.5 (entry 4, Table 1) to 30 mL (entry 18, Table 1) of ethanol, the selectivity toward alcohols does not change, being stable around 89%. We have also carried out the reaction while varying the quality of starting ethanol (see Table S1), establishing that the performances of the process are also satisfying when employing real matrixes, meaning that although a range in yield and selectivity can be detected, catalyst **1** is not deactivated by water or other feedstock impurities.

Overall, at the best reaction conditions (0.02 mol % loading of **1**, 20 mol % loading of sodium ethoxide, and T = 150°C; entry 13 in Table 1), the conversion of ethanol is 50%, and the selectivity to total alcohols is >99%.

To obtain further insights into the reaction behavior, the time-evolving product distribution has been experimentally studied at selected reaction conditions (i.e., 0.2 mol % loading of **1**, 20 mol % loading of sodium ethoxide, and T = 150°C; entry 4 in Table 1). We selected these reaction conditions instead of the best one, as weighting an extremely low amount of catalyst is challenging.

As shown in Table 2 (and Figure 5), ethanol conversion is 21% with 95% alcohol selectivity after 15 min (entry 1, Table 2). The turnover frequency (TOF) is calculated to be 400 h^{-1} at that time. The rate of the reaction levels off after ca. 4 h, and we consider the reaction to be finished. In fact, if the reaction was carried out for 8 h

Please cite this article in press as: Calcagno et al., Combined computational-experimental study of Ru(0)-catalyzed Guerbet reaction, Cell Reports Physical Science (2024), https://doi.org/10.1016/j.xcrp.2024.102291

Table 3. Guerbet reaction on 1-butanol

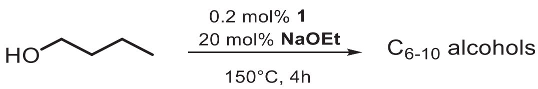

Entry	1 (mol %)	NaOEt (mol %)	BuOH (mL)	Time (h)	T (°C)	Conversion BuOH (%)	Yield ($C_{6\text{-}10}$) (%)	C-loss (%)	Selectivity ($C_{6\text{-}10}$) (%)
1	0.2	20	0.5	4	150	33	33	0	>99
2	0.2	10	0.5	4	150	21	16	5	76

The conversion of 1-butanol, the yield and selectivity of products, and the carbon loss are reported with different reaction conditions.

in the same conditions (entry 7, Table 2), then we found that the conversion of ethanol increases by only 5 pt.% compared to after 4 h.

As the reaction proceeds, the selectivity to total alcohols decreases to 89% at 4 h and 84% at 8 h (entries 6 and 7, Table 2). As mentioned before, this trend could be ascribed to the formation of uncharacterized long-chain alcohols and to the side processes. The presence of C_N long-chain alcohols is in line with the increasing selectivity to $C_{6\text{-}10}$ alcohol over time, which is 14% at 15 min and increases up to 21% at 4 h and 28% at 8 h (entries 6 and 7, Table 2). Importantly, 1-butanol is the main product of the process at all reaction times, while subsequent homologation products ($C_{6\text{-}10}$) are 23% of total alcohols at the end of the Guerbet reaction. Notably, a significant increase of pressure is observed during the reaction. Gas chromatography (GC) analyses of the reaction mixture provided evidence for the production of a large amount of molecular hydrogen in the final headspace of the reaction vessel (29% yield at 4 h; Table 2). The time-evolving amount of molecular hydrogen follows a trend similar to the yield of alcohols, suggesting the presence of an energetically competitive molecular hydrogen evolution side process in parallel with the homologation.[23,25]

Not surprisingly, the catalytic system performs well even if 1-butanol is used as the starting reactant instead of ethanol (entry 1, Table 3). The results reported in Table 3 confirm the detrimental behavior of a lower NaOEt loading on substrate conversion (33% with 20 mol % base vs. 21% with 10 mol %) and selectivity (>99% vs. 77%).

It is noteworthy that the proposed catalytic system **1**/NaOEt shows a similar performance to the previously reported ruthenium and iridium complexes working under the same reaction conditions,[10–16] while this is the first example that exploits an NHC moiety as the ligand. This functionalization improves the stability of the transition metal complex, paving the way to recycle the catalyst. Preliminary recycling tests carried out at the selected reaction conditions (entry 4, Table 1) showed that catalyst **1** can indeed be reused after removing all the alcohols under vacuum and refilling fresh EtOH and NaOEt, leading to a conversion of 45% and a yield of alcohols of 29%. The recycling of ruthenium molecular catalysts active in the Guerbet reaction has been previously reported.[13,14,43] In all these reports, the catalyst maintained the activity. Nevertheless, in the latest work reported by Schaub and co-workers,[43] the system maintains good activity even without the need for an additional base in the second cycle, with a generally better performance. Therefore, it becomes essential to understand catalyst **1** activation and the Ru(0)-catalyzed Guerbet reaction mechanism in the presence of an NHC ligand that allows regeneration of the stable pre-catalysts.

Activation of the catalyst and dehydrogenation of ethanol

The ruthenium(0)-NHC complex **1** is a pre-catalytic species, as the metal center must have a vacancy in its valence to promote the reaction. There are two possible activation

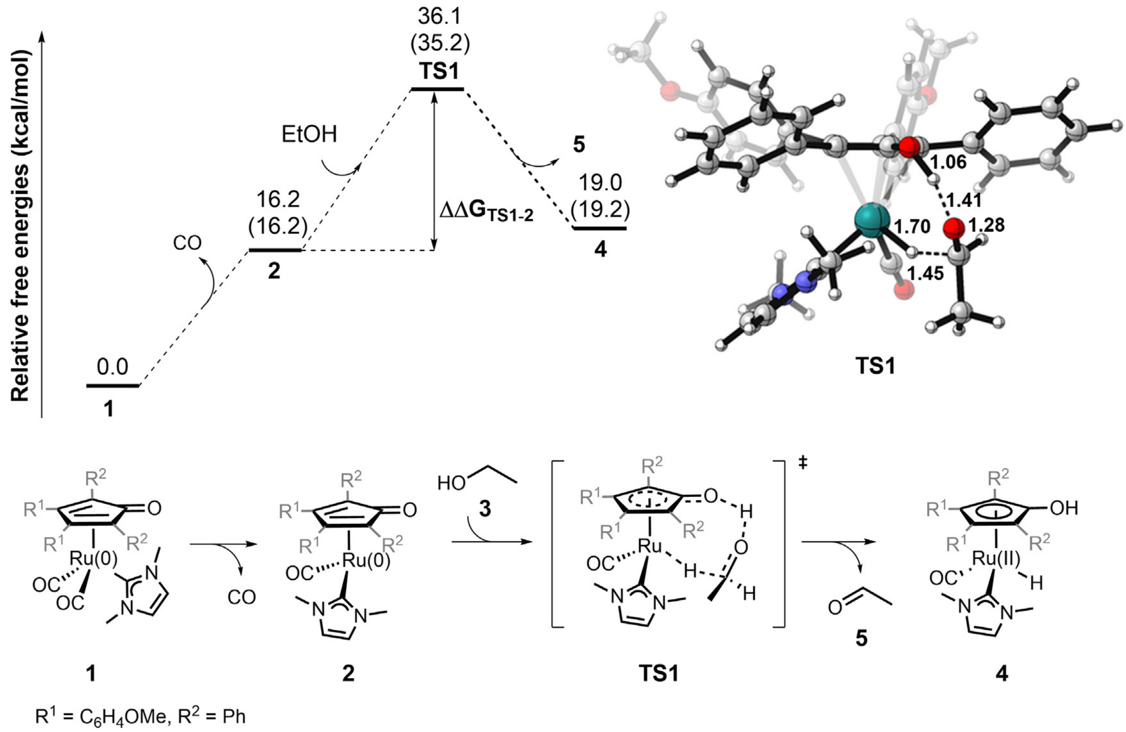

Figure 1. Activation of the catalyst and dehydrogenation of acetaldehyde

Calculated free energy profile (top left) for the activation of the pre-catalyst (**1**) and the dehydrogenation of ethanol (**3**) to acetaldehyde (**5**) by the activated catalyst (**2**). The energies reported are calculated at B3LYP-D3/6-311+G(2d,2p)/LANL2DZ/PCM(ethanol)//B3LYP/6-31G(d,p)/LANL2DZ and B3LYP-D3/6-311+G(2d,2p)/LANL2DZ/PCM(ethanol)//B3LYP-D3/6-31G(d,p)/LANL2DZ/PCM(ethanol) (in brackets) levels of theory. The species involved in these reaction steps are also reported (bottom). On the top right, the geometry of **TS1** optimized at B3LYP/6-31G(d,p)/LANL2DZ level of theory is reported.

mechanisms, involving the dissociation of one of the CO ligands or the carbene ligand. The DFT calculations (see the supplemental information for computational details) show that the dissociation of CO from **1** resulting in active species **2** costs 16.2 kcal/mol, while the dissociation of NHC costs 27.4 kcal/mol (see Figure S4).

Species **2** (Figure 1) is a bifunctional metal-ligand dehydrogenation catalyst, as the ruthenium center and the CpO ligand can cooperate via an internal redox process by accepting a hydride and proton, respectively. The calculations show that the dehydrogenation of ethanol (**3**) to acetaldehyde (**5**) catalyzed by **2** follows a concerted outer-sphere mechanism[44] with an overall barrier of 36.1 kcal/mol (**TS1**; Figure 1) with respect to **1**. It is worth noticing that the transition state is chiral, as the metal has three different ligands, and the ethanol is prochiral. This leads to two diastereomeric transition states (**TS1** and **TS2**) differing by 0.7 kcal/mol, resulting in the hydrogenated catalyst **4** and acetaldehyde **5** as products (see Figure S5). Species **4** is also chiral, as the ruthenium center is bonded to four different ligands (Figure 1).

We have also considered the dehydrogenation mechanism starting from the complex in which the NHC ligand has dissociated, but this mechanism has a calculated barrier that is 7.9 kcal/mol higher than **TS1**, thus ruling out this possibility (see Figure S4). These results are also in line with previous work by Mazzoni and coworkers.[13] Namely, the complex with the dissociated NHC ligand is the dehydrogenated monomer of the Shvo's catalyst, which was already established as being inactive in the Guerbet reaction in the same conditions reported in the present work.[13]

To evaluate the influence of the solvent and the dispersion effects during geometry optimizations on these DFT results, we first compared the minimum energy pathways (MEPs) for catalyst activation using gas-phase-optimized geometries of the stationary points (i.e., at the B3LYP/6-31G(d,p)/LANL2DZ level) or including solvent and dispersion corrections (i.e., at the B3LYP-D3/6-31G(d,p)/LANL2DZ/PCM(ethanol) level; see the supplemental information for computational details). As reported in Figure 1, the two optimization methods returned quite similar energetics. The gas-phase-optimization feature reduced computational costs, and thus, since the number of stationary points increases significantly in the subsequent reaction steps (due to the involvement of geometric isomers and the conformational analysis), only these computations are discussed in detail in the following sections unless otherwise specified. Anyway, a comprehensive analysis of geometry optimizations including solvent and the dispersion effects is reported in the supplemental information for the energetics of the ethanol to 1-butanol homologation reaction (see Tables S3 and S4; Scheme S5), showing that the choice of the optimization method does not affect the characterization of the Guerbet reaction mechanism. Despite some sizable effects on the energetics of a few elementary steps, these do not involve rate-determining processes, overall yielding minor changes in the kinetic network simulations (see Tables S5 and S6; Figures S11 and S12) of the overall homologation to higher alcohols (i.e., 1-butanol and 1-hexanol).

To experimentally confirm that the dissociation of CO occurs preferentially, we carried out GC analysis of the headspace gases of the reaction vessel and ^{13}C-labeling NMR experiments. With GC analysis, we detected CO in the headspace of the reactor. Furthermore, we carried out the Guerbet reaction for 1 h under a pressurized ^{13}CO atmosphere and using not-isotopically labeled **1** (see the supplemental information for details). ^{13}C-NMR analysis of the final reaction mixture shows an unambiguous enrichment of **1** by the labeled carbon monoxide (see Figure S2), confirming the exchange of this ligand during the catalytic process.

C–C coupling via base-catalyzed aldol condensation

The acetaldehyde **5** produced in the previous step is involved in an off-cycle C–C coupling process via aldol condensation catalyzed by sodium ethoxide (**6**).[26] This reaction step is central in the overall mechanism since it leads to unsaturated C_4 ketones that are involved in both the formation of the 1-butanol product **16** and subsequent homologations to higher alcohols (Figure 2).

The calculations show that the acetaldehyde is first enolized to **7** with an activation barrier of 14.4 kcal/mol (**TS3**) (see Figure 2). Then, enolate **7** reacts with another molecule of **5**, forming sodium 4-oxobutan-2-olate (**8**). For this reaction step, we have not been able to locate the corresponding transition state in the gas phase. Therefore, to have an estimation of the height of the energy barrier, we have recomputed this step at the B3LYP-D3/6-311+G(2d,2p)/LANL2DZ/PCM(ethanol)//B3LYP-D3/6-31G(d,p)/LANL2DZ/PCM(ethanol) level of theory. In this way, we have characterized the corresponding transition state, which lies at 13.0 kcal/mol (see the supplemental information for details). According to this value, this elementary step cannot be rate determining, and its inclusion/omission does not imply any change in the following interpretation of the overall reaction mechanism.

Since the elimination of a water molecule is required to complete the condensation, **8** is then protonated to 3-hydroxybutanal **9**, which is then involved in the last two steps of the condensation. As shown in Figure 2, the deprotonation involves the two enantiotropic hydrogens of the methylene group of **9** and leads

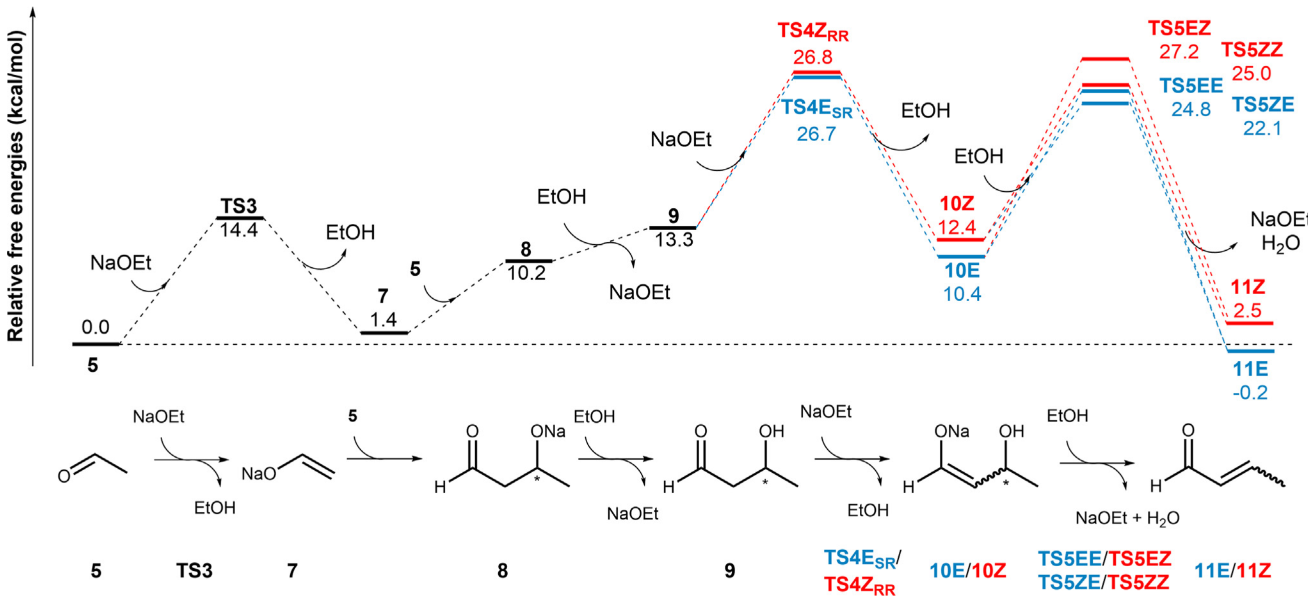

Figure 2. Aldol condensation

Calculated free energy profiles for the base-catalyzed aldol condensation of two molecules of acetaldehyde (**5**) to (*E/Z*)-crotonaldehyde (**11E**/**11Z**) at the B3LYP-D3/6-311+G(2d,2p)/LANL2DZ/PCM(ethanol)//B3LYP/6-31G(d,p)/LANL2DZ level of theory. The species involved in the reaction steps are shown on the bottom.

to two geometric isomers of the resulting enolate, i.e., **10E**/**10Z**. For this step, eight asymmetric transition states can be located, i.e., four for each C=C configuration. Since for each C=C configuration, two pairs of transition states are enantiomers (i.e., **TS4E$_{RR}$** and **TS4E$_{SS}$** and **TS4E$_{RS}$** and **TS4E$_{SR}$** for the *E* configuration), only the diastereomeric transition states RR and SR have been investigated for both the *E* and the *Z* configurations. The calculations show that the **TS4E$_{SR}$** and **TS4Z$_{RR}$** are the lowest in energy and differ by only 0.1 kcal/mol (**TS4E$_{SR}$** = 26.7 kcal/mol and **TS4Z$_{RR}$** = 26.8 kcal/mol), but the enolate product **10E** is lower in energy than **10Z** by 2.0 kcal/mol.

In the following reaction step, water elimination occurs, yielding to final products (*E/Z*)-crotonaldehyde (**11E**/**11Z**) via deprotonation of a molecule of ethanol and restoring the base co-catalyst. During this step, there is a migration of the C=C bond (see Figure 2), implying that both **10E** and **10Z** can lead to either **11E** or **11Z**, according to different conformations of the methyl in the transition states (i.e., **TS4EE**, **TS4EZ**, **TS4ZE**, and **TS4ZZ**, where the first (E/Z) letter refers to the configuration of the C=C bond in the reagent and the second (E/Z) letter refers to the configuration of the C=C bond in the product).

The calculations show that the lowest energy pathways to reach **11E** and **11Z** both start from **10Z** (**TS5ZE** = 22.1 kcal/mol and **TS5ZZ** = 25.0 kcal/mol). Interestingly, the calculations indicate that **TS5ZE** and **TS5ZZ** follow a stepwise mechanism, while **TS5EE** and **TS5EZ** follow a concerted one. As shown in Figure 2, deprotonation of **9** (**TS4Z$_{RR}$** = 26.8 kcal/mol) is the rate-determining step of the aldol condensation.

Hydrogenation of crotonaldehyde and homologation to higher alcohols

Following the aldol condensation step, we have calculated the double hydrogenation of crotonaldehyde (**11E**/**11Z**) to 1-butanol (**16**) catalyzed by two molecules of the hydrogenated catalyst **4** (Scheme 2). Notably, at least 16 competing hydrogenation

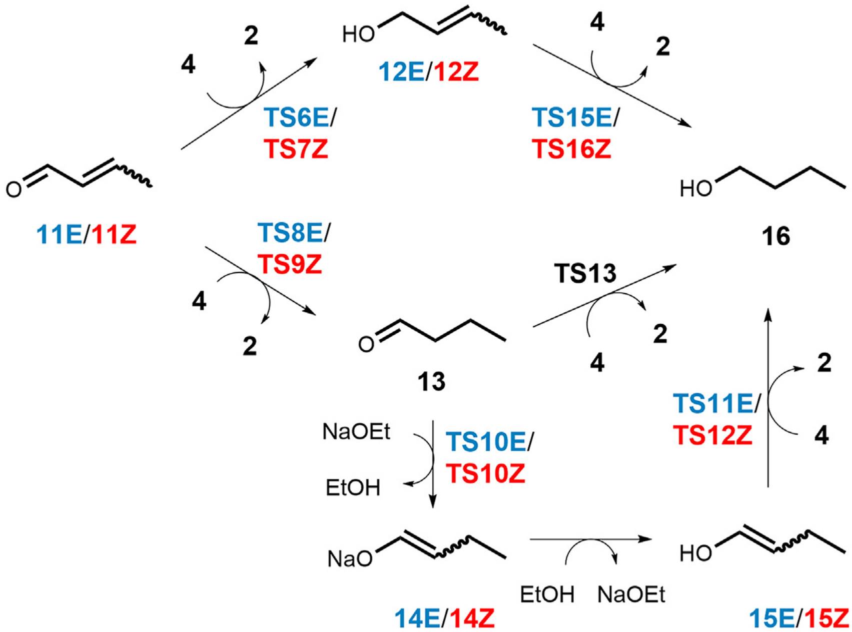

Scheme 2. Competitive hydrogenation pathways suggested by DFT calculations

pathways are possible for this step. In fact, the hydrogenations of the C=C and the C=O bonds happen following an unknown order,[26] two geometrical isomers of the reactant are present, and species **4** is chiral, implying diastereomeric catalyst-substrate interactions according to each prochiral face of each double bond.

We have characterized all these pathways, but only the energies of the lowest diastereomeric transition states will be discussed here. As shown in Scheme 2 and Figure 3, according to different hydrogenation orders, different intermediates are formed. If C=C is the first bond to be reduced, then 1-butanal **13** would be formed from both geometric isomers of **11**. This elementary step is exergonic by 11.3 kcal/mol, and the energy barriers are found to be 21.2 kcal/mol for **TS8E** and 23.7 kcal/mol for **TS9Z**. If C=O is the first bond to be reduced, then either the *E*- or *Z*-crotyl alcohol (**12E**/**12Z**) is formed from the corresponding geometric isomer of (*E*/*Z*)-crotonaldehyde. The C=O reduction is more favored by 2.6–3.4 kcal/mol (**TS6E** = 18.6 kcal/mol and **TS7Z** = 20.3 kcal/mol) with respect to that of the C=C bond, but it is thermodynamically disfavored, being slightly exergonic ($\Delta\Delta G_{12Z\text{-}11Z}$ = 0.2 kcal/mol and $\Delta\Delta G_{12E-11E}$ = 1.7 kcal/mol). Conversely, the energy barriers for the second hydrogenation to 1-butanol (**15**) are much higher for the (*E*/*Z*)-crotyl alcohol (**TS15E** = 33.4 kcal/mol and **TS16Z** = 33.8 kcal/mol) than for 1-butanal (**TS13** = 5.1 kcal/mol). However, before drawing conclusions about the preferred hydrogenation mechanism, we also investigated the keto-enol tautomerism between 1-butanal **13** and its tautomers (*E*/*Z*)-1-butene-1-ol (**15E**/**15Z**) in order to examine whether there is an energetically competitive pathway that could open to a third hydrogenation mechanism. As in the first step of the C–C coupling, sodium ethoxide (**6**) takes a proton in the β position of **13**'s carbonyl, forming the corresponding enolates (**14E**/**14Z**) through two isomeric transition states (**TS10E** = 2.9 kcal/mol and **TS10Z** = 3.2 kcal/mol). Then, the molecule of ethanol (**3**) formed during the previous step protonates **14E**/**14Z** to form **15E**/**15Z**. The overall base-catalyzed tautomerism is lower in energy than the hydrogenation of **13** (i.e., **TS13**) by 2.2 kcal/mol for the *E* tautomer (**TS10E**) and 1.9 kcal/mol for the *Z* one (**TS10Z**).

CellPress
OPEN ACCESS

Cell Reports
Physical Science
Article

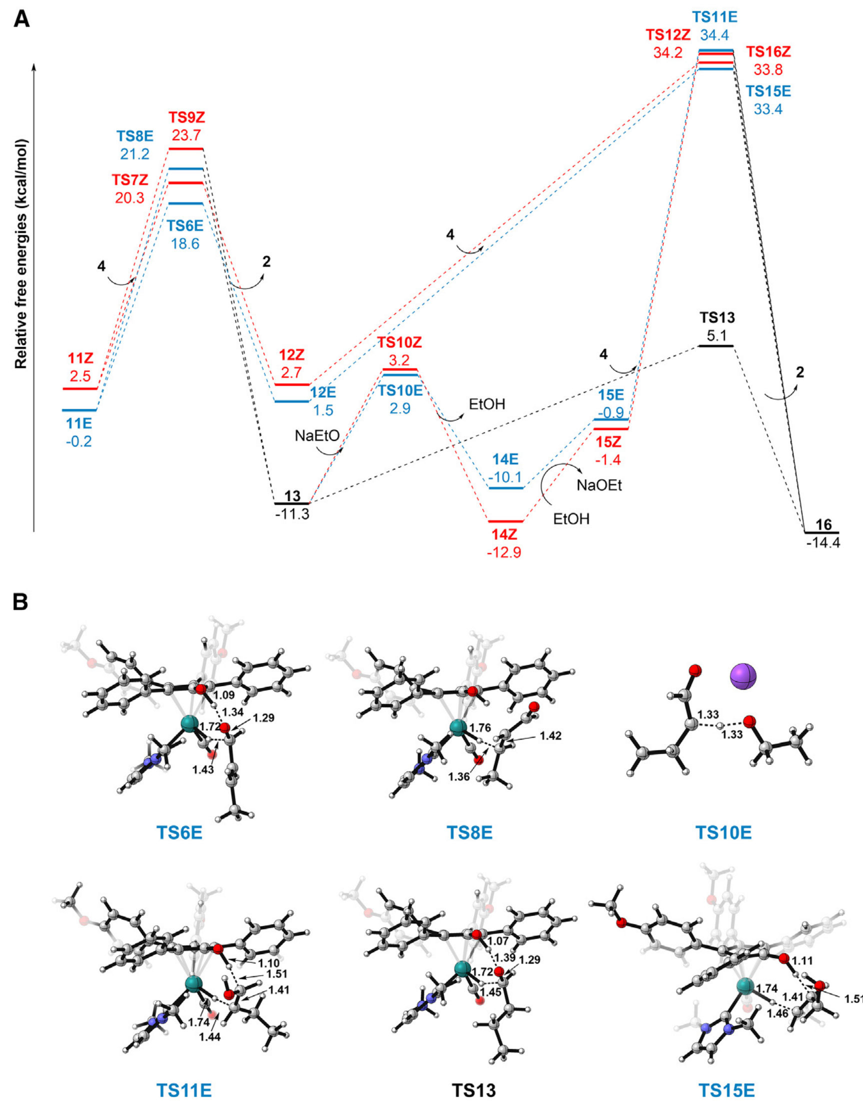

Figure 3. Hydrogenation of (*E*/*Z*)-crotonaldehydes

(A) Calculated free energy profiles for the double hydrogenation of (*E*/*Z*)-crotonaldehydes (**11E**/**11Z**) to 1-butanol (**16**) at the B3LYP-D3/6-311+G(2d,2p)/LANL2DZ/PCM(ethanol)//B3LYP/6-31G(d,p)/LANL2DZ level of theory.

(B) Optimized structures of selected transition states involved in the hydrogenation process of **11E**/**11Z** to **16**.

Since the tautomerism is energetically accessible, we have calculated the energy barriers to hydrogenate **15E**/**15Z** to **16**. The energies of the corresponding transition states (**TS11E** = 34.4 kcal/mol and **TS12Z** = 34.2 kcal/mol) are comparable to the those computed to reduce **12E**/**12Z** (i.e., **TS15E**/**TS16Z**), being much higher than **TS13**. Therefore, the double-hydrogenation mechanism of **11E**/**11Z** comprises a first reduction of the C=C bond to reach **13**, followed by the hydrogenation of the C=O bond (see Figure 3).

With the aim of experimentally verifying the preferred hydrogenation pathway of **11E**/**11Z**, we carried out the Guerbet reaction for 15 min and analyzed the reaction mixture at that time with GC-mass spectrometry (MS). Among all possible intermediates, we found only species **13** (see Figure S3). This outcome is in line with computational predictions, confirming that the C=C bond of **11E**/**11Z** is the first one to be reduced.

Please cite this article in press as: Calcagno et al., Combined computational-experimental study of Ru(0)-catalyzed Guerbet reaction, Cell Reports Physical Science (2024), https://doi.org/10.1016/j.xcrp.2024.102291

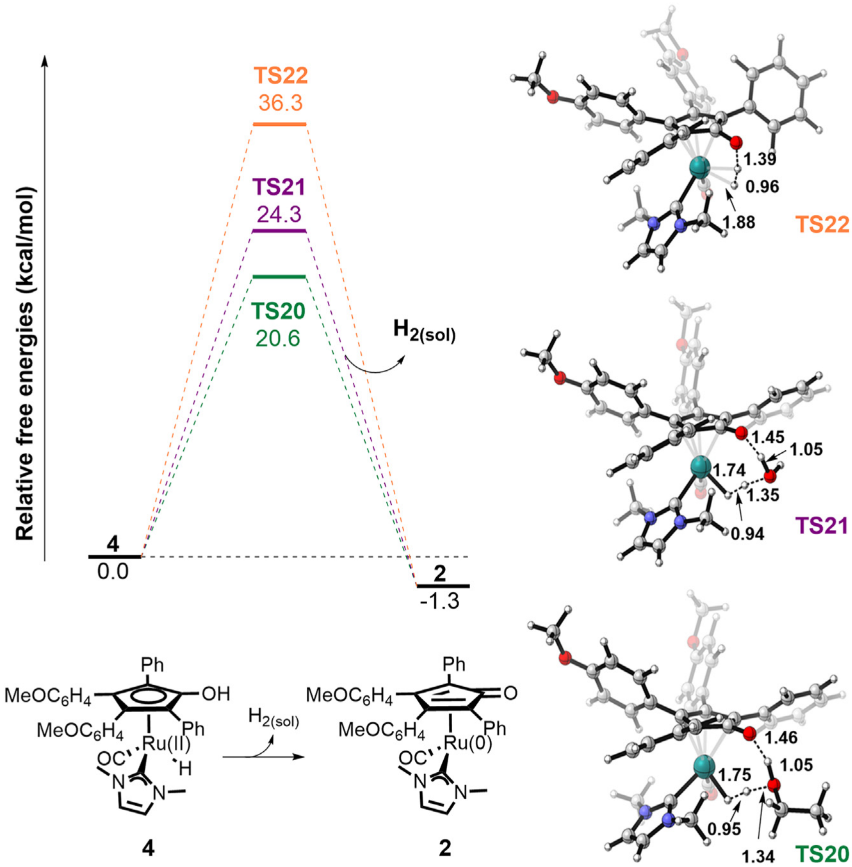

Figure 4. Hydrogen evolution

Computed free energy profiles (top left) for the molecular hydrogen evolution process and optimized geometries (right) of related transition states at the B3LYP-D3/6-311+G(2d,2p)/LANL2DZ/PCM(ethanol)//B3LYP/6-31G(d,p)/LANL2DZ level of theory. The species involved in this reaction step are shown on the bottom left.

Up to this point, we have characterized the key steps of the Guerbet reaction for the homologation of ethanol (**3**) to its first homologation product, 1-butanol **16**. However, the experimental product distribution shows that homologation to higher alcohols, especially the C_6 ones, is not completely negligible (Table 2). Therefore, for completeness and to obtain a more detailed picture of the Guerbet reaction, we have also fully characterized the homologation of 1-butanol to 1-hexanol **25**. As expected, the reaction scheme is almost the same as that already described for **3** (see section S5.3 reported in the supplemental experimental procedures for further details).

Evolution of molecular hydrogen

Next, we investigated the process of molecular hydrogen evolution. The hydrogenated catalyst **4** can generate and release an H_2 molecule via internal proton-hydride coupling processes. For this step, we have compared three possible reaction pathways: (1) direct proton-hydride coupling and proton shuttle mechanisms assisted by a molecule of either (2) water or (3) ethanol. As shown in Figure 4, the direct pathway has an energy barrier of 36.3 kcal/mol (**TS22**), which is much higher than those of the assisted pathways, in which water and ethanol behave as proton relay groups with barriers of 24.3 and 20.6 kcal/mol, respectively.[45]

Interestingly, the value of **TS20** is comparable to the height of the hydrogenation processes involving (*E/Z*)-crotonaldehyde to 1-butanal (see Figure 3A). This indicates that when the hydrogenated catalyst **4** is formed, there is a competition between the first reduction of **11E**/**11Z** and the molecular hydrogen evolution process. The calculations are thus in line with the experimental outcome, as the final amount of molecular hydrogen is not negligible with respect to the alcohols (yield [H_2] = 29%, yield [$C_{4\text{-}10}$] = 47%; see Table 2) and the time evolution is similar for all these species.

Interestingly, in a very recent study conducted by Shaub and co-workers,[43] it was reported that hydrogen pressure could be beneficial for the Guerbet reaction. For example, a Milstein-type complex loaded at 0.01 mol % under T = 180°C, t = 2 h, and NaOEt = 6 mol % conditions performed better in terms of EtOH conversion (15% vs. 41%) and BuOH yield (7% vs. 29%) when a H_2 pre-reaction partial pressure of 10 bar was employed. To verify if a similar effect was also possible for catalyst **1**, we tested the influence of the hydrogen pressure on the catalytic performance. To increase and control the pressure, further reactions were performed in a 50 mL stainless-steel autoclave. Comparing the results under 10 bar of N_2 or H_2 (conditions: 5 mL EtOH, 20 mol % NaOEt, and 0.02 mol % catalyst **1**, 150°C, 4 h), a detrimental effect in the presence of H_2 pressure was detected. In fact, the reaction under N_2 performs with a conversion in line with that in the Schlenck bomb (Table 1, entry 8), although with a slightly higher carbon loss (conversion: 62%; $C_{4\text{-}10}$ yield: 45%), while under H_2, a significant drop in conversion is observed (34%; $C_{4\text{-}10}$ yield: 31%), with good selectivity. The same reaction at 20 bar H_2 showed a slight decrease in conversion (31%), which goes along with a significant drop in selectivity ($C_{4\text{-}10}$ yield: 8%).

To conclude, the results suggest a strong correlation between the hydrogen evolution side process and the homologation of alcohols when catalyst **1** is employed. In fact, the H_2 evolution step is strictly dependent on the chemical properties of **1** and is promoted by ethanol, which is the reactant (and the solvent) of the Guerbet reaction. This is a fundamental insight for future improvements to the performance of the Guerbet reaction.

Overall reaction mechanism and kinetic simulations

The DFT calculations shed light on the complexity of the mechanism of the homologation of ethanol to 1-butanol and 1-hexanol via the Guerbet reaction. Scheme 3 summarizes the overall reaction mechanism of the homologation of ethanol to 1-butanol as obtained by the current work. The Ru(0)-NHC complex catalyzes the hydrogen transfer processes, while the base co-catalyzes the off-cycle C–C coupling reaction, which leads to two different (*E/Z*) configurational pathways. Moreover, the evolution of molecular hydrogen interferes with the hydrogen transfer cycle, further complicating the reaction network. The interconnections within the cycle further increase when the homologation to 1-hexanol is considered (see Scheme S4). In fact, multiple alcoholic (or ketonic) intermediates are potential reactants for further homologations (e.g., **13** is directly involved in the homologation to 1-hexanol).

In general, in DFT studies of catalytic reactions, it is often possible to extract information about conversions, yields, and selectivities by analyzing the computed free energy profiles. However, when the catalytic cycles are complex—e.g., when different processes happen in parallel, multiple catalysts cooperate, and there are many interconnections between intermediates—as in the present case, microkinetic simulations are very valuable in order to obtain information about the distribution

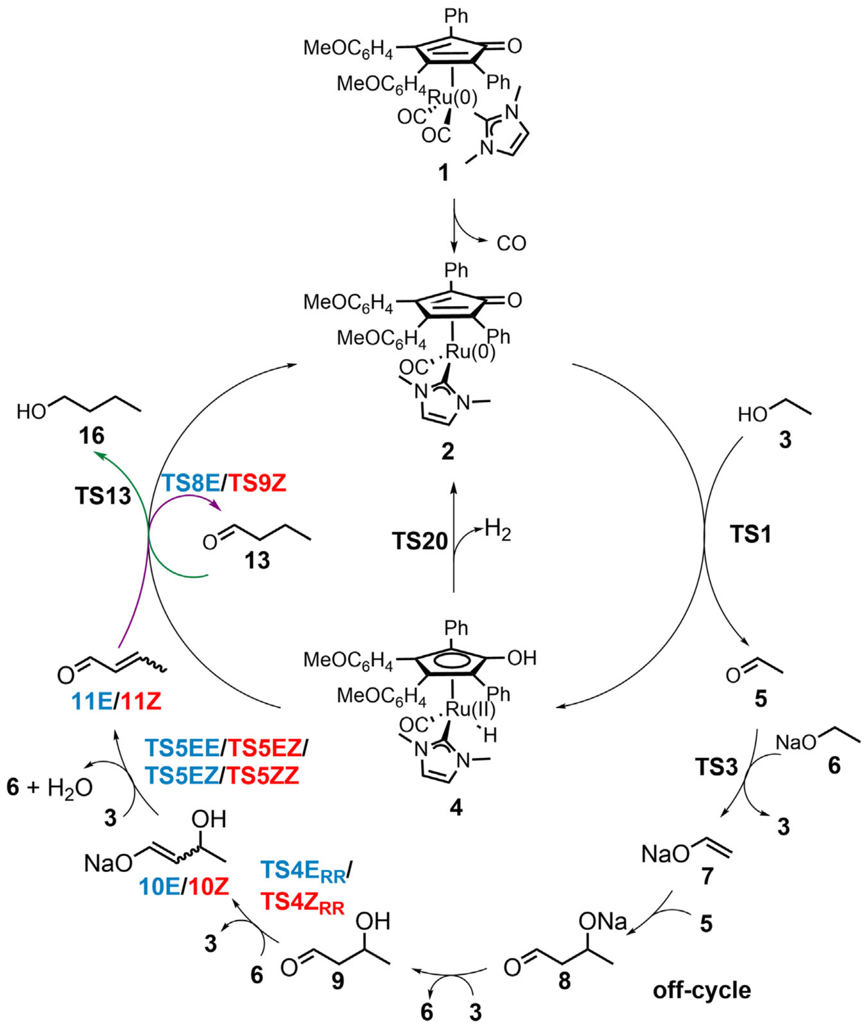

Scheme 3. The overall catalytic mechanism of the Guerbet reaction characterized in this work

of products. Numerical kinetics simulations make it possible to directly compare free energy profiles computed at the DFT level with experimental observations, giving insights into the key reaction steps governing yields and selectivities.[46,47]

In the present work, a kinetic network has been set up consisting of all the elementary steps reported in Schemes 3 and S4. Two additional equilibria not discussed above have also been considered in the kinetic network. Namely, the molecular hydrogen obtained from the proton-hydride coupling (TS20) is released in solution, so it must be involved in a solution-gas equilibrium, and the sodium ethoxide must be in equilibrium with ethanol according to an acid-base equilibrium with water, which is the co-product of the aldol condensation. Approximations to both these equilibria have been added to the kinetic network, as discussed in the supplemental information.

We have performed kinetic simulations using the experimental initial concentrations of the ethanol, the sodium ethoxide, and catalyst 1. The simulations were run for 4 h, which is the reaction time selected for the experiments, as discussed above.

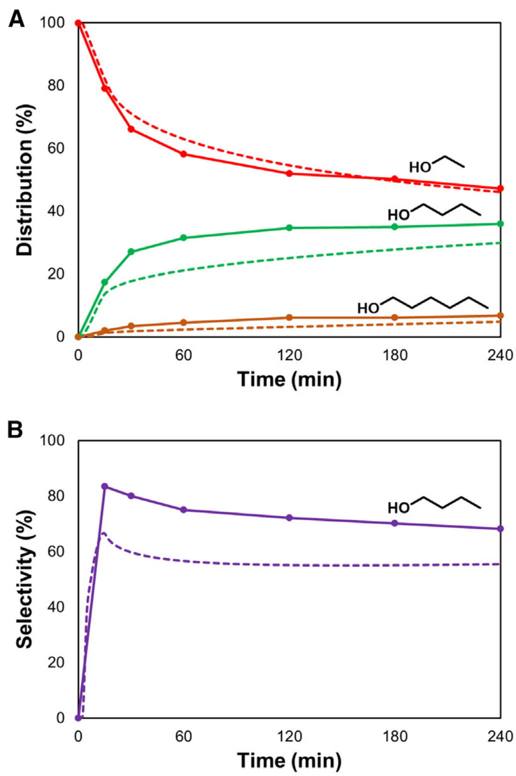

Figure 5. Simulated and experimental product and selectivity time-evolving distributions

(A) Experimental (solid lines) and simulated (dashed lines) time-evolving ethanol conversion and distribution of products. Residual ethanol (in red) and yields of 1-butanol (in green) and 1-hexanol (in brown) are reported.

(B) Experimental (solid lines) and simulated (dashed lines) selectivity to 1-butanol. Initial concentrations: $[\mathbf{1}]_0$ = 0.03424 mol/L, $[EtOH]_0$ = 17.12 mol/L, and $[NaOEt]_0$ = 3.287 mol/L.

Gratifyingly, we find good agreement between the experimental and simulated time evolutions of the alcohols (see Figure 5). For example, the conversion of ethanol after 4 h (experimental 53% vs. simulated 54%), the yield of 1-butanol (36% vs. 30%), the yield of 1-hexanol (7% vs. 5%), and the yield of molecular hydrogen (29% vs. 33%) are all well reproduced (see Figure 5). The yield of 1-butanol is generally slightly underestimated, leading to lower selectivity (experimental: 68%, simulated: 56% after 4 h).

Kinetic simulations also gave insights into the reason why the reaction stops at about a 30% yield of 1-butanol. The higher the yield of alcoholic products, the higher the concentration of water formed during aldol condensation. When water is formed, it reacts with NaOEt according to the acid/base equilibrium [$NaOEt + H_2O \leftrightharpoons EtOH + NaOH$] (see the supplemental information for details). This makes the concentration of the co-catalyst drop down and thus hampers the overall reaction. This finding agrees with the experimental trend observed for the loading of the co-catalyst: when the concentration of NaOEt is lowered, the conversion of EtOH decreases (Table 1).

Notably, when considering geometries optimized with solvent and dispersion corrections, the theoretical results are essentially confirmed, with product distribution at the end of the reaction slightly improved if compared with experimental data (see Figure S12).

Table 4. Simulated product distribution and selectivity to alcohols

Entry	1 (mol %)	NaOEt (mol %)	Simulation time (h)	Conversion EtOH (%)	Yield BuOH (%)	Yield alcohols[a] (%)	Selectivity alcohols (%)
1	0.2	20	4	54	30	35	65
2	0.2	20	8	62	35	43	69
3	0.02	20	4	51	28	32	63
4	0.02	10	4	42	13	15	36
5	0.02	5	4	36	11	12	33
6	0.01	10	4	39	16	18	46
7	0.01	5	4	32	10	10	31

The simulated conversion of ethanol, the yield of 1-butanol, and the yield and selectivity of alcohols are reported with various reaction conditions. The temperature is 150°C in all simulations.
[a]The total yield of alcohols is the sum of the yields of 1-butanol and 1-hexanol.

To further examine the validity of the calculations and the kinetic model, we carried out more kinetic simulations while varying the reaction conditions, such as the starting concentrations and the reaction time, following some of the experimental conditions listed in Table 1. The results are given in Table 4.

The kinetic model reproduces the trends related to the variation of concentration of NaOEt base co-catalyst **6** quite well. Keeping catalyst **1** loading constant and decreasing the concentration of **6** leads to a decrease of each of the ethanol conversions, the yield of 1-butanol, and the selectivity (see Table 4, entry 3 vs. entries 4 and 5).

When the concentration of NaOEt (**6**) is kept constant and the loading of **1** is varied, the kinetic model reproduces well that the yield of 1-butanol decreases when the concentration of **1** is lowered (entries 1, 3, 4, and 6, Table 4). However, the model does not reproduce the fact that the conversion of the ethanol decreases with the increase of the loading of **1** except for 5 mol % loading of the base, which shows the opposite trend (entries 4 and 6, Table 4). This discrepancy with respect to experiments can be ascribed to the fact that the kinetic model does not consider the Tishchenko and Cannizzaro reactions explicitly, which are likely responsible for this trend.

Finally, the model also reproduces the trends of the conversion of ethanol and the total yield of alcohols due to longer reaction times (entry 1 vs. 2, Table 4). However, the model does not reproduce the experimental observation that the concentration of 1-butanol decreases in going from 4 to 8 h. Instead, the simulations show that the concentration increases (entry 1 vs. 2, Table 4), which is reasonably due to the approximation of the consecutive homologations involving 1-butanol in our model, as homologations of 1-hexanol and higher alcohols were not considered.

To summarize, we find generally good correspondence between the experimental observations and simulated kinetics. It should be remembered that at the temperature of the experiments, an error of 1.94 kcal/mol in the calculated barrier implies a 10-fold change in the associated rate constant. Considering this, the agreement is satisfactory, and the kinetic simulations provided thus strongly support the reaction mechanism proposed on the basis of the DFT calculations (Scheme 3).

To gain further insights into the mechanism and factors influencing the overall rate and selectivity of the reaction, we carried out more kinetic simulations in which the barriers of the selected steps were modified by $\pm$1.94 kcal/mol. As discussed above, the mechanism of the Guerbet reaction established in the present work can be

Table 5. Sensitivity analysis

		+1.94 kcal/mol					−1.94 kcal/mol				
Entry	Modified TS	Conversion EtOH (%)	Yield BuOH (%)	Yield alcohols[a] (%)	Yield H_2 (%)[b]	Selectivity alcohols (%)	Conversion EtOH (%)	Yield BuOH (%)	Yield alcohols[a] (%)	Yield H_2 (%)[b]	Selectivity alcohol (%)
1	none	54	30	35	33	65	54	30	35	33	65
2	activation of **1**	43	23	27	33	63	59	37	44	28	75
3	**TS1**	52	27	33	33	63	54	30	35	33	65
4	**TS4Z$_{RR}$**	51	26	32	33	63	62	39	42	34	68
5	**TS8E/TS9Z**[c]	43	10	12	50	28	56	34	43	25	77
6	**TS20**	38	34	40	15	105[d]	54	31	34	34	63

The effect of modifications of selected energy barriers on product distribution after 4 h at 150°C is reported. Initial concentrations in the simulations: $[\mathbf{1}]_0$ = 0.03424 mol/L, $[EtOH]_0$ = 17.12 mol/L, and $[NaOEt]_0$ = 3.287 mol/L.

[a]The total yield of alcohols is the sum of the yields of 1-butanol and 1-hexanol.

[b]Since the sol/gas equilibrium for molecular hydrogen is considered, the yield of H_2 is the computed total concentration, i.e., $H_{2(sol)}$+ $H_{2(gas)}$.

[c]Energies of both transition states are modified.

[d]Note that this value is higher than 100% because the selectivity is computed using the yield and conversion values calculated with respect to the initial concentration of the ethanol, i.e., $[EtOH]_0$ = 1 equiv. However, its real concentration is somewhat larger since the sodium ethoxide reacts with water and is converted to ethanol during the Guerbet reaction.

divided into five stages: (1) activation of the catalyst, (2) dehydrogenation of ethanol (Figure 2), (3) C–C coupling (Figure 3A), (iv) hydrogenation of the C–C coupling product (Figure 4), and (5) molecular hydrogen evolution process (Figure 5). We have selected the rate-determining step of each of these five stages for the kinetics analysis, and the results are given in Table 5.

The cost of the activation of catalyst **1** has an impact on the overall product distribution (entry 2, Table 5). When the activation energy of **1** is increased, the reaction is slowed down, i.e., the conversion is lower. Interestingly, the selectivity to total alcohols is almost the same (entry 2 vs. 1, Table 5), while the selectivity to molecular hydrogen increases from 61% to 77%. Conversely, when the energy cost of the activation is lowered (entry 2, Table 5), the performance of the reaction is improved, and the selectivity to molecular hydrogen decreases to 47%. This outcome suggests that the activation of catalyst **1** is a key step governing the reaction performance and the impact of the undesired production of molecular hydrogen, as any change in the energy of this step will have a direct influence on the overall barrier of the reaction.

Interestingly, when the barrier for the dehydrogenation of ethanol (**TS1**) is increased, the reaction slows down, while nothing happens to the reaction performance when the barrier is decreased (entry 3, Table 5). This outcome shows that the dehydrogenation of ethanol constitutes one of the rate-determining steps, as when its barrier is lowered, another barrier takes over, and no change is observed in the rate.

The simulations showed that the hydrogenation of (*E*/*Z*)-crotonaldehyde strongly influences the reaction outcome (entry 5, Table 5). When the energies of **TS8E**/**TS9Z** are raised by 1.94 kcal/mol, the yield of 1-butanol decreases from 54% to 43%, and the selectivity to total alcohols decreases from 65% to 28%. On the other hand, the yield of the molecular hydrogen increases from 33% to 50% (entry 5, Table 5). When the energies of **TS8E**/**TS9Z** are lowered, the overall performance of the reaction improves, and the yield of molecular hydrogen decreases (entry 5, Table 5). This outcome further corroborates the hypothesis of the direct competition and anti-correlation between the hydrogenation of (*E*/*Z*)-crotonaldehyde and the molecular hydrogen evolution.

A similar behavior is observed when the energy of $\mathbf{TS4Z_{RR}}$ is modified (entry 4, Table 5). When this barrier is lowered, the performance of the Guerbet reaction improves, with a lower impact on the evolution of molecular hydrogen (entry 4, Table 5). On the other hand, when the energy of $\mathbf{TS4Z_{RR}}$ is increased, the conversion of ethanol decreases, with no variation in the yield of molecular hydrogen (entry 4, Table 5). Therefore, calculations also show that the aldol condensation step indirectly governs the evolution of molecular hydrogen. This can be ascribed to the fact that the reaction rate of the first hydrogenation step depends on the concentration of **11E**/**11Z**, and the larger the rate constant of the aldol condensation, the larger the concentration of **11E**/**11Z** and, thus, the reaction rate of the hydrogenation.

Finally, the role of molecular hydrogen evolution was investigated (entry 6, Table 5). When the energy of **TS20** is increased by 1.94 kcal/mol, the conversion of ethanol decreases to 38%, with a positive impact on the selectivity to total alcohols, which becomes 105% (entry 6, Table 4). Note here that this value is higher than 100% because the selectivity is computed using the yield and the conversion values calculated with respect to the initial concentration of the ethanol, i.e., $[EtOH]_0$ = 1 equiv. However, in addition to the starting ethanol, at 4 h, the majority of the sodium ethoxide co-catalyst is converted to ethanol during the reaction according to its acid/base equilibrium (see the supplemental information for details), which means that the total available concentration of the ethanol is higher than its starting concentration.

This response to the energy of **TS20** suggests that when the evolution of molecular hydrogen is suppressed, a larger concentration of the hydrogenated catalyst **4** is involved in the hydrogenation of the organic intermediates instead of producing molecular hydrogen. However, quite surprisingly, if the step of molecular hydrogen evolution is totally removed from the kinetic model, then the Guerbet reactions does not take place at all after 4 h. This result shows that the evolution of molecular hydrogen is not an innocent side process but a regulatory step that ensures the proper turnover of active catalyst **2**. In fact, the hydrogenation steps are slower than the dehydrogenation of ethanol (Figures 1 and 3A).

If **4** is not converted back to **2** by releasing an equivalent of molecular hydrogen, then the amount of ethanol that is converted to acetaldehyde **5** is low, and the hydrogenation reaction does not proceed, nor is **2** restored. On the other hand, when evolution barrier **TS20** is lowered by 1.94 kcal/mol, no noticeable variations are recorded (entry 6, Table 5), suggesting that it is no longer rate determining, as already discussed for **TS1**.

DISCUSSION

In the present study, we have established the reaction mechanism for the homologation of ethanol to higher alcohols via the Guerbet reaction using a combined experimental-computational approach. The reaction is carried out in the presence of a ruthenium(0)-NHC catalyst, which has not been used before for this reaction, and sodium ethoxide as a base co-catalyst.

We have characterized the detailed reaction mechanism of the homologation of ethanol to 1-butanol and 1-butanol to 1-hexanol, showing that the overall process involves a dehydrogenation/hydrogenation cycle performed by the metal catalyst, an off-cycle aldol condensation catalyzed by sodium ethoxide, and a molecular hydrogen evolution step.

The dehydrogenation/hydrogenation cycle is switched on when the organoruthenium catalyst is activated by the release of one ligand. DFT calculations predict that the dissociation of the carbon monoxide ligand is preferred over the carbene one, indicating that the active catalyst features a bound NHC ligand. Experimental ^{13}C-NMR investigations have shown that the CO ligand has a high exchange rate, corroborating the computational prediction.

Next, metal-catalyzed ethanol dehydrogenation forms acetaldehyde, which enters into an off-cycle base-catalyzed aldol condensation, yielding α,β-unsaturated aldehydes and water. Then, the aldehydic products enter back in the Ru catalyst cycle to be doubly hydrogenated. This final step converts the α,β-unsaturated intermediates to the final alcoholic product. The hydrogenation process features a complex network of reactions. Namely, there are multiple competitive pathways involving geometrical isomers of α,β-unsaturated reactants, different hydrogenation orders, keto-enol tautomerism, and diastereomeric transition states. Among various possibilities, DFT calculations revealed that the preferred pathway comprises a first reduction of the C=C bond, followed by the direct hydrogenation of the C=O bond. In the case of 1-butanol production, experimental GC-MS analysis showed that only the 1-butanal intermediate could be found in the reaction mixture, confirming the computational prediction (see Figure S3).

Upon the formation of the alcohol products, the side evolution of molecular hydrogen was established by experimental GC analysis. The DFT calculations demonstrate that molecular hydrogen comes from an internal proton-hydride coupling of the hydrogenated metal catalyst. This process is assisted by a molecule of ethanol via a proton-shuttling mechanism. Since it features an energy barrier like the hydrogenation of the α,β-unsaturated intermediates, this reaction step interferes with the hydrogen-borrowing cycle, producing molecular hydrogen and restoring the dehydrogenated catalyst.

Since the Guerbet reaction is an intricate process featuring a complex reaction mechanism, we carried out microkinetic simulations to compare the experimental and computational outcomes. The simulations showed good agreement with experimental data, providing support to the reaction mechanism proposed in the present work.

Based on our kinetic simulations, general strategies to improve the performance of the Guerbet reaction can be suggested, such as (1) lowering the cost for activation of the metal catalyst, (2) employing more efficient base co-catalysts to reduce the energy cost of the aldol condensation, (3) enhancing the hydrogenation performance of the catalyst, and (5) controlling the molecular hydrogen evolution to modulate the organometallic catalyst turnover.

The present synergistic computational-experimental study provides an unprecedented mechanistic understanding of the Guerbet reaction and, thus, paves the way for further developments of homogeneous catalysts for more efficient upgrading of ethanol to 1-butanol and higher alcohols.

EXPERIMENTAL PROCEDURES

Details regarding experimental procedures can be found in the supplemental experimental procedures.

RESOURCE AVAILABILITY

Lead contact

Further information and requests for resources should be directed to and will be fulfilled by the lead contact, Dr. Ivan Rivalta (i.rivalta@unibo.it).

Materials availability

All other data supporting the findings of this study are available within the article and supplemental information.

Data and code availability

The complete experimental and computational procedures are provided in the supplemental information. Cartesian coordinates of DFT optimized stationary points have been deposited in a freely available dataset at https://doi.org/10.6092/unibo/amsacta/7842.

ACKNOWLEDGMENTS

I.R. gratefully acknowledges the use of HPC resources of the "Pôle Scientifique de Modélisation Numérique" (PSMN) of the ENS de Lyon, France. Part of this work was financed by the European Union - NextGenerationEU through the Italian Ministry of University and Research under PNRR "Piano Nazionale di Ripresa e Resilienza" - Mission 4 "Istruzione e Ricerca," Component 2 "Dalla ricerca all'impresa," Investment 1.1, "Fondo per il Programma Nazionale di Ricerca e Progetti di Rilevante Interesse Nazionale (PRIN) – Piano Nazionale di Ripresa e Resilienza, addressed to Progetti di Ricerca di Rilevante Interesse Nazionale," D.D. no. 104 del 2/2/2022, project title: Biomass-derived alcohols and polyols valorisation and use by dehydrogenation/hydrogenation reactions promoted by bifunctional and proton-responsive homogeneous catalysts (ALCOVAL)," codice 20225N5T5B – CUP J53D23008500006. F.H. thanks the Swedish Research Council (2019-04010) for financial support.

AUTHOR CONTRIBUTIONS

Conceptualization, R.M., I.R., and F.H.; investigation, F.C. and C.C.; validation, A.G., A.M., C.C., and F.C.; autoclave experiments on the effect of H_2 pressure, A.P.; writing – original draft, F.C. and C.C.; writing – review & editing, F.C., C.C., R.M., F.H., and I.R.; resources, F.T., R.M., I.R., and M.G.; supervision, R.M., I.R., and F.H.

DECLARATION OF INTERESTS

The authors declare no competing interests.

SUPPLEMENTAL INFORMATION

Supplemental information can be found online at https://doi.org/10.1016/j.xcrp.2024.102291.

Received: July 1, 2024
Revised: August 20, 2024
Accepted: October 21, 2024
Published: November 13, 2024

REFERENCES

1. Guerbet, M. (1899). Action de l'alcool amylique de fermentation sur son dérivé iodé.

2. Guerbet, M. (1909). Condensation de l'alcool isopropylique avec son dérivé sodé; formation du méthylisobutylcarbinol et du diméthyl-2.4-heptanol-6. CR Acad. Sci. Paris *149*, 129–132.

3. Angelici, C., Weckhuysen, B.M., and Bruijnincx, P.C.A. (2013). Chemocatalytic Conversion of Ethanol into Butadiene and Other Bulk Chemicals. ChemSusChem *6*, 1595–1614. https://doi.org/10.1002/cssc.201300214.

4. Campos-Fernández, J., Arnal, J.M., Gómez, J., and Dorado, M.P. (2012). A comparison of performance of higher alcohols/diesel fuel blends in a diesel engine. Appl. Energy *95*, 267–275. https://doi.org/10.1016/j.apenergy.2012.02.051.

5. Torres, G.M., Frauenlob, R., Franke, R., and Börner, A. (2015). Production of alcohols via hydroformylation. Catal. Sci. Technol. *5*, 34–54. https://doi.org/10.1039/C4CY01131G.

6. Kozlowski, J.T., and Davis, R.J. (2013). Heterogeneous Catalysts for the Guerbet Coupling of Alcohols. ACS Catal. *3*, 1588–1600. https://doi.org/10.1021/cs400292f.

7. Aitchison, H., Wingad, R.L., and Wass, D.F. (2016). Homogeneous Ethanol to Butanol Catalysis—Guerbet Renewed. ACS Catal. *6*, 7125–7132. https://doi.org/10.1021/acscatal.6b01883.

8. Messori, A., Gagliardi, A., Cesari, C., Calcagno, F., Tabanelli, T., Cavani, F., and Mazzoni, R. (2023). Advances in the homogeneous catalyzed alcohols homologation: the mild side of the Guerbet reaction. A mini-review. Catal. Today *423*, 114003. https://doi.org/10.1016/j.cattod.2023.01.010.

9. Gabriëls, D., Hernández, W.Y., Sels, B., Van Der Voort, P., and Verberckmoes, A. (2015). Review of catalytic systems and thermodynamics for the Guerbet condensation reaction and challenges for biomass valorization. Catal. Sci. Technol. *5*, 3876–3902. https://doi.org/10.1039/C5CY00359H.

10. Chakraborty, S., Piszel, P.E., Hayes, C.E., Baker, R.T., and Jones, W.D. (2015). Highly Selective Formation of n-Butanol from Ethanol through

the Guerbet Process: A Tandem Catalytic Approach. J. Am. Chem. Soc. *137*, 14264–14267. https://doi.org/10.1021/jacs.5b10257.

11. Dowson, G.R.M., Haddow, M.F., Lee, J., Wingad, R.L., and Wass, D.F. (2013). Catalytic Conversion of Ethanol into an Advanced Biofuel: Unprecedented Selectivity for n-Butanol. Angew. Chem., Int. Ed. Engl. *52*, 9005–9008. https://doi.org/10.1002/anie.201303723.

12. Tseng, K.-N.T., Lin, S., Kampf, J.W., and Szymczak, N.K. (2016). Upgrading ethanol to 1-butanol with a homogeneous air-stable ruthenium catalyst. Chem. Commun. *52*, 2901–2904. https://doi.org/10.1039/C5CC09913G.

13. Mazzoni, R., Cesari, C., Zanotti, V., Lucarelli, C., Tabanelli, T., Puzzo, F., Passarini, F., Neri, E., Marani, G., Prati, R., et al. (2018). Catalytic Biorefining of Ethanol from Wine Waste to Butanol and Higher Alcohols: Modeling the Life Cycle Assessment and Process Design. ACS Sustain. Chem. Eng. *7*, 224–237. https://doi.org/10.1021/acssuschemeng.8b02959.

14. Cesari, C., Gagliardi, A., Messori, A., Monti, N., Zanotti, V., Zacchini, S., Rivalta, I., Calcagno, F., Lucarelli, C., Tabanelli, T., et al. (2022). Boosting the guerbet reaction: A cooperative catalytic system for the efficient bio-ethanol refinery to second-generation biofuels. J. Catal. *405*, 47–59. https://doi.org/10.1016/j.jcat.2021.11.027.

15. Davies, A.M., Li, Z.-Y., Stephenson, C.R.J., and Szymczak, N.K. (2022). Valorization of Ethanol: Ruthenium-Catalyzed Guerbet and Sequential Functionalization Processes. ACS Catal. *12*, 6729–6736. https://doi.org/10.1021/acscatal.2c01570.

16. Xie, Y., Ben-David, Y., Shimon, L.J.W., and Milstein, D. (2016). Highly Efficient Process for Production of Biofuel from Ethanol Catalyzed by Ruthenium Pincer Complexes. J. Am. Chem. Soc. *138*, 9077–9080. https://doi.org/10.1021/jacs.6b05433.

17. Fu, S., Shao, Z., Wang, Y., and Liu, Q. (2017). Manganese-Catalyzed Upgrading of Ethanol into 1-Butanol. J. Am. Chem. Soc. *139*, 11941–11948. https://doi.org/10.1021/jacs.7b05939.

18. Kulkarni, N.V., Brennessel, W.W., and Jones, W.D. (2018). Catalytic Upgrading of Ethanol to n-Butanol via Manganese-Mediated Guerbet Reaction. ACS Catal. *8*, 997–1002. https://doi.org/10.1021/acscatal.7b03653.

19. Ohligschläger, A., van Staalduinen, N., Cormann, C., Mühlhans, J., Wurm, J., and Liauw, M.A. (2021). The Guerbet Reaction Network – a Ball-in-a-Maze-Game or: Why Ru-MACHO-BH is Poor in Coupling two Ethanol to n-Butanol. Chemistry. Methods. *1*, 181–191. https://doi.org/10.1002/cmtd.202000056.

20. Zhang, Q., Dong, J., Liu, Y., Wang, Y., and Cao, Y. (2016). Towards a green bulk-scale biobutanol from bioethanol upgrading. J. Energy Chem. *25*, 907–910. https://doi.org/10.1016/j.jechem.2016.08.010.

21. Chieregato, A., Velasquez Ochoa, J., Bandinelli, C., Fornasari, G., Cavani, F., and Mella, M. (2015). On the Chemistry of Ethanol on Basic Oxides: Revising Mechanisms and Intermediates in the Lebedev and Guerbet reactions. ChemSusChem *8*, 377–388. https://doi.org/10.1002/cssc.201402632.

22. Ho, C.R., Shylesh, S., and Bell, A.T. (2016). Mechanism and Kinetics of Ethanol Coupling to Butanol over Hydroxyapatite. ACS Catal. *6*, 939–948. https://doi.org/10.1021/acscatal.5b02672.

23. Veibel, S., and Nielsen, J.I. (1967). On the mechanism of the Guerbet reaction. Tetrahedron *23*, 1723–1733. https://doi.org/10.1016/S0040-4020(01)82571-0.

24. Bradley, D.C., Mehrotra, R.C., Rothwell, I.P., and Singh, A. (2001). 2 - Homometallic Alkoxides. In Alkoxo and Aryloxo Derivatives of Metals, D.C. Bradley, R.C. Mehrotra, I.P. Rothwell, and A. Singh, eds. (Academic Press), pp. 3–181. https://doi.org/10.1016/B978-012124140-7/50002-5.

25. Sponholz, P., Mellmann, D., Cordes, C., Alsabeh, P.G., Li, B., Li, Y., Nielsen, M., Junge, H., Dixneuf, P., and Beller, M. (2014). Efficient and selective hydrogen generation from bioethanol using ruthenium pincer-type complexes. ChemSusChem *7*, 2419–2422. https://doi.org/10.1002/cssc.201402426.

26. Rawat, K.S., Mandal, S.C., Bhauriyal, P., Garg, P., and Pathak, B. (2019). Catalytic upgrading of ethanol to n-butanol using an aliphatic Mn–PNP complex: theoretical insights into reaction mechanisms and product selectivity. Catal. Sci. Technol. *9*, 2794–2805. https://doi.org/10.1039/C9CY00501C.

27. Huang, F., Liu, Z., and Yu, Z. (2016). C-Alkylation of Ketones and Related Compounds by Alcohols: Transition-Metal-Catalyzed Dehydrogenation. Angew. Chem., Int. Ed. Engl. *55*, 862–875. https://doi.org/10.1002/anie.201507521.

28. Obora, Y. (2014). Recent Advances in α-Alkylation Reactions using Alcohols with Hydrogen Borrowing Methodologies. ACS Catal. *4*, 3972–3981. https://doi.org/10.1021/cs501269d.

29. Dobereiner, G.E., and Crabtree, R.H. (2010). Dehydrogenation as a Substrate-Activating Strategy in Homogeneous Transition-Metal Catalysis. Chem. Rev. *110*, 681–703. https://doi.org/10.1021/cr900202j.

30. Reed-Berendt, B.G., Latham, D.E., Dambatta, M.B., and Morrill, L.C. (2021). Borrowing Hydrogen for Organic Synthesis. ACS Cent. Sci. *7*, 570–585. https://doi.org/10.1021/acscentsci.1c00125.

31. Piazzi, A., Tabanelli, T., Gagliardi, A., Cavani, F., Cesari, C., Cespi, D., Passarini, F., Conversano, A., Viganò, F., Di Bona, D., and Mazzoni, R. (2023). Molecular catalysed Guerbet reaction: Moving to the larger and the Greener through LCA and scale up simulation approaches. Sustain. Chem. Pharm. *35*, 101222. https://doi.org/10.1016/j.scp.2023.101222.

32. Kim, J.-H., Kim, J.-W., Shokouhimehr, M., and Lee, Y.-S. (2005). Polymer-Supported N-Heterocyclic Carbene−Palladium Complex for Heterogeneous Suzuki Cross-Coupling Reaction. J. Org. Chem. *70*, 6714–6720. https://doi.org/10.1021/jo050721m.

33. Boztepe, C., Künkül, A., Yaşar, S., and Gürbüz, N. (2018). Heterogenization of homogeneous NHC-Pd-pyridine catalysts and investigation of their catalytic activities in Suzuki-Miyaura coupling reactions. J. Organomet. Chem. *872*, 123–134. https://doi.org/10.1016/j.jorganchem.2018.07.004.

34. Cesari, C., Conti, S., Zacchini, S., Zanotti, V., Cassani, M.C., and Mazzoni, R. (2014). Sterically driven synthesis of ruthenium and ruthenium–silver N-heterocyclic carbene complexes. Dalton Trans. *43*, 17240–17243. https://doi.org/10.1039/C4DT02747G.

35. Hopkinson, M.N., Richter, C., Schedler, M., and Glorius, F. (2014). An overview of N-heterocyclic carbenes. Nature *510*, 485–496. https://doi.org/10.1038/nature13384.

36. Peris, E. (2018). Smart N-Heterocyclic Carbene Ligands in Catalysis. Chem. Rev. *118*, 9988–10031. https://doi.org/10.1021/acs.chemrev.6b00695.

37. Cesari, C., Cingolani, A., Parise, C., Zacchini, S., Zanotti, V., Cassani, M.C., and Mazzoni, R. (2015). Ruthenium hydroxycyclopentadienyl N-heterocyclic carbene complexes as transfer hydrogenation catalysts. RSC Adv. *5*, 94707–94718. https://doi.org/10.1039/C5RA18345F.

38. Cesari, C., Mazzoni, R., Müller-Bunz, H., and Albrecht, M. (2015). Ruthenium(0) complexes with triazolylidene spectator ligands: Oxidative activation for (de)hydrogenation catalysis. J. Organomet. Chem. *793*, 256–262. https://doi.org/10.1016/j.jorganchem.2015.02.022.

39. Cesari, C., Mazzoni, R., Matteucci, E., Baschieri, A., Sambri, L., Mella, M., Tagliabue, A., Basile, F.L., and Lucarelli, C. (2019). Hydrogen Transfer Activation via Stabilization of Coordinatively Vacant Sites: Tuning Long-Range π-System Electronic Interaction between Ru(0) and NHC Pendants. Organometallics *38*, 1041–1051. https://doi.org/10.1021/acs.organomet.8b00850.

40. Balaraman, E., Khaskin, E., Leitus, G., and Milstein, D. (2013). Catalytic transformation of alcohols to carboxylic acid salts and H2 using water as the oxygen atom source. Nat. Chem. *5*, 122–125. https://doi.org/10.1038/nchem.1536.

41. Zhang, L., Nguyen, D.H., Raffa, G., Trivelli, X., Capet, F., Desset, S., Paul, S., Dumeignil, F., and Gauvin, R.M. (2016). Catalytic Conversion of Alcohols into Carboxylic Acid Salts in Water: Scope, Recycling, and Mechanistic Insights. ChemSusChem *9*, 1413–1423. https://doi.org/10.1002/cssc.201600243.

42. Gusev, D.G., and Spasyuk, D.M. (2018). Revised Mechanisms for Aldehyde Disproportionation and the Related Reactions of the Shvo Catalyst. ACS Catal. *8*, 6851–6861. https://doi.org/10.1021/acscatal.8b01153.

43. Jungfer, M.R., Schwarz, J.L., Rominger, F., Oeser, T., Paciello, R., Hashmi, A.S.K., and Schaub, T. (2024). H_2 Pressure Dependence in the Homogeneously Catalyzed Guerbet Reaction of Ethanol to Butanol using Mn(I) and Ru(II). ChemCatChem *16*, e202301588. https://doi.org/10.1002/2Fcctc.202301588.

44. Comas-Vives, A., Ujaque, G., and Lledós, A. (2007). Hydrogen Transfer to Ketones

Catalyzed by Shvo's Ruthenium Hydride Complex: A Mechanistic Insight. Organometallics *26*, 4135–4144. https://doi.org/10.1021/om7004832.

45. Casey, C.P., Johnson, J.B., Singer, S.W., and Cui, Q. (2005). Hydrogen Elimination from a Hydroxycyclopentadienyl Ruthenium(II) Hydride: Study of Hydrogen Activation in a Ligand−Metal Bifunctional Hydrogenation Catalyst. J. Am. Chem. Soc. *127*, 3100–3109. https://doi.org/10.1021/ja043460r.

46. Kalek, M., and Himo, F. (2017). Mechanism and Selectivity of Cooperatively Catalyzed Meyer–Schuster Rearrangement/Tsuji–Trost Allylic Substitution. Evaluation of Synergistic Catalysis by Means of Combined DFT and Kinetics Simulations. J. Am. Chem. Soc. *139*, 10250–10266. https://doi.org/10.1021/jacs.7b01931.

47. Besora, M., and Maseras, F. (2018). Microkinetic modeling in homogeneous catalysis. WIREs Comput. Mol. Sci. *8*, e1372. https://doi.org/10.1002/wcms.1372.